Acta Astronautica 176 (2020) 558–566

Contents lists available at ScienceDirect

Acta Astronautica

journal homepage: www.elsevier.com/locate/actaastro

Research Paper

Air-LUSI: Development of a pointing and tracking control system for lunar spectral measurements

Andrew Newton [a], Andrew Cataford [a], Stephen E. Maxwell [b], S. Andrew Gadsden [a,*], Kevin Turpie [c]

[a] College of Engineering, University of Guelph, Guelph, Ontario, N1G 2W1, Canada
[b] Remote Sensing Group, Sensor Science Division, National Institute of Standards and Technology, Gaithersburg, MD, 20899, United States of America
[c] Joint Center for Earth Systems Technology, University of Maryland, Baltimore County, Baltimore, MD, 21228, United States of America

A B S T R A C T

The airborne lunar spectral irradiance mission is an inter-agency partnership between the US National Aeronautics and Space Administration and the US National Institute of Standards and Technology that aims to make SI-traceable measurements of lunar spectral irradiance at visible to near-infrared wavelengths with unprecedented accuracy. This information is vital to using the Moon as a calibration source for Earth observing satellites. To minimize uncertainty, the lunar measurements are made above 90% of the Earth's atmosphere from an Earth Resources 2 aircraft, a civilian descendant of the U-2 spy plane. Situated in a large wing pod, a custom-designed telescope automatically tracks the Moon and the measurements are fed into a spectrometer. This information is being used to develop an extremely accurate model that can be used to calibrate satellites. An Engineering Flight Campaign was completed in August 2018 and a Demonstration Flight Campaign in November 2019, which demonstrated autonomous lunar acquisition and tracking as well as measurements of the Moon's spectral irradiance from an altitude of approximately 21 km. This article presents the simplified double gimbal control system design that was used to manipulate the telescope, and was capable of targeting the Moon with a root mean squared tracking error of about 0.1°.

1. Introduction

The air-LUSI mission continues efforts to establish the Moon as a calibration source for Earth observing satellites [1–6]. It is a partnership between the US National Aeronautics and Space Administration (NASA) and the US National Institute of Standards and Technology (NIST), collaborating with the US Geological Survey (USGS), the University of Maryland Baltimore County, and the University of Guelph in Ontario, Canada. The primary mission objective is to acquire measurements of lunar spectral irradiance with unprecedented accuracy. With this improved knowledge of the Moon, the accuracy of Earth observing satellites can be improved, contributing to better remote sensing capabilities of the orbiting radiometric sensors responsible for monitoring the health of our planet. The accuracy of previous, ground-based work aimed at characterizing the radiometric properties of the Moon has suffered in part because of atmospheric absorption. To improve lunar spectral irradiance (LUSI) measurement accuracy, one must reduce the affects of the atmosphere and enforce rigorous calibration controls. Air-LUSI solves the first problem by measuring from a high-altitude, airborne platform, NASA's ER-2 aircraft — a civilian descendent of the U-2 spy plane. At altitudes up to 21 km, LUSI measurements are captured above 95% of the Earth's atmosphere, thereby reducing the effects of scattering and absorption. The second problem is solved by deploying NIST-maintained radiometric artifacts to the ER-2 hangar for pre- and post-flight calibration, as well as by incorporating on-board radiometric validation sources in the measurement system.

The airborne instrument includes the IRradiance Instrument Subsystem (IRIS), which includes a spectrometer connected to a telescope and was designed and built by NIST using a commercially available spectrometer. The IRIS telescope is maneuvered from a stow position to a zenith view port, acquires and locks onto the Moon for measurement, and then moves back to the stow position when the observations are complete. To facilitate the telescope movement and lunar tracking, air-LUSI uses its Autonomous Robotic TElescope Mount Instrument Subsystem (ARTEMIS). A team at the University of Guelph developed ARTEMIS to use a double gimbal, allowing the system to freely move in azimuth and elevation [7]. Linear actuators were used as a variable length linkages to induce rotation about each degree of freedom [8–10]. The ARTEMIS control system uses a simplified approach to control the pointing of the telescope when compared to other inertially stabilized systems that are commonly implemented for target tracking [11]. The simplified system treats both the azimuth and elevation axes as completely independent degrees of freedom and implements two distinct single input single output controllers for both axes. The control system

* Corresponding author.
E-mail addresses: anewto03@uoguelph.ca (A. Newton), acatafor@uoguelph.ca (A. Cataford), stephen.maxwell@nist.gov (S.E. Maxwell), gadsden@uoguelph.ca (S.A. Gadsden), kturpie@umbc.edu (K. Turpie).

https://doi.org/10.1016/j.actaastro.2020.07.004
Received 2 June 2020; Received in revised form 30 June 2020; Accepted 2 July 2020
Available online 6 July 2020

Nomenclature

AFRC	Armstrong Flight research Center
Air-LUSI	Airborne Lunar Spectral Irradiance Mission
ARTEMIS	Autonomous Robotic Telescope Mount Instrument Subsystem
DAQ	Data Acquisition System
ER-2	Earth Resources 2 Aircraft
FoV	Field of View
IRIDIUM	Iridium Satellite Constellation
IRIS	Irradiance Instrument Subsystem
JSON	JavaScript Object Notation
LoS	Line of Sight
LUSI	Lunar Spectral Irradiance
NASA	National Aeronautics and Space Administration
NASDAT	NASA Airborne Science Data and Telemetry System
NIST	National Institute of Standards and Technology
NTP	Network Time Protocol
OpenCV	Open Source Computer Vision Library
PID	Proportional Integral Derivative Controller
RMSE	Root Mean Squared Error
ROS	Robotic Operating System
UDP	User Datagram Protocol
USGS	US Geological Survey
UTC	Universal Coordinated Time

relied entirely on the data obtained from a machine vision tracking camera which performed simplified image processing techniques to extract targeting information while keeping sampling rates high and overall delay low [12–14].

A typical target tracking system will implement a gimbal assembly that allows the orientation of a payload to be adjusted in multiple degrees of freedom. Generally, gimbal assemblies use a set of bearings and shafts to provide freedom of motion while actuators adjust the systems pointing in each degree of freedom. The majority of pointing and tracking problems use a double gimbal that consists of an outer gimbal that can adjust the azimuth degree of freedom and an inner gimbal to adjust the elevation [15–18].

Most published work describing the solution for the control problem at hand pertains to Inertially Stabilized Control Units. Pointing and tracking problems are commonly found within munitions systems, air and land craft surveillance systems, communications, and astronomy. Although all systems perform similar tasks, their control system design can vary depending on the intended operating environment and whether the targeting system is stationary or moving. All pointing and tracking problems implement some form of Line of Sight (LoS) controller for each degree of freedom, however, robust systems that are deployed on moving vehicles also implement Inertially Stabilized Platform controllers [15–21].

The first general approach when developing a tracking system is to have a basic Line of Sight (LoS) controller. These controllers are often referred to as 'visual servoing' controllers because they interpret the distance separating a target from a desired location within an image frame. Based on the separation between the current and desired location of the target, the system will write correcting commands to move the system and align the target with a given setpoint [12,13,19–22]. The LoS controllers are generally considered a low frequency control loop that manages the majority of the pointing and tracking requirements while the inertially stabilized control units implement a high frequency inner control loop for rejecting disturbances caused by the relative motion of the system carrier. This method of control compensates for the extended processing times of LoS vision control systems and maintains pointing position relative to the global coordinate system [15,17].

This article presents the simplified double gimbal control system design that is used for ARTEMIS, and is capable of targeting the Moon with a root mean squared tracking error of about $0.1°$. The system implements a visual servo controller. The paper is organized as follows: Section 2 describes the design and constraints, Section 3 describes the computer vision system that was developed, and Section 4 summarizes the camera and telescope alignment process. The developed pointing controllers and mode of network communication is described in Sections 5 and 6, respectively. The system performance during the Demonstration Flight Campaign is discussed in Section 7, followed by concluding remarks.

2. Design and constraints

The ARTEMIS enables air-LUSI to autonomously acquire and track the Moon with the IRIS telescope through a zenith view port. Its robotic design mounts the telescope on a double gimbal, with the outer gimbal facilitating movement in azimuth and the inner gimbal providing changes in elevation. For the robotic telescope to meet the requirements of the mission, the control system is designed to allow for seamless integration with the ER-2 aircraft as well as interpret commands from the pilot.

The robotic telescope controller of the air-LUSI system is therefore required to operate as a state machine, that occupies an idle state while the aircraft is ascending to its lunar tracking station, and then transitions to a tracking state once the aircraft has reached the desired heading and altitude. NASA's ER-2 aircraft has four designated pilot switches (R1–R4) in the cockpit that give the pilot bare-minimum in-flight control of the instrument. During nominal operation, these switches are the only inputs that initiate transitions between data acquisition and tracking states [23]. Inter-subsystem communications are discussed in more detail in Section 6.

The ER-2 flight plan during observations is determined by: the need to keep the IRIS telescope aperture unoccluded by the wing pod aperture (which limits viewing to a minimum of 46.7° above horizontal and ±15° from a direction orthogonal to the direction of flight); by the limits of motion of the elevation controller (about 80° above horizontal); by the need to minimize the amount of atmosphere between the telescope and the moon; and, by the requirement that direct or scattered sunlight cannot influence the measurement. The requirements combine to prefer night-time observations when the moon is near transition, when it crosses the local meridian and reaches its zenith. At this time, the moon's azimuthal angle is directly south of the observations from the northern hemisphere, and a flight-line from east to west centers the wing pod aperture and the telescope's azimuthal motion on the moon. The duration of observations is chosen so that good statistics can be achieved on the spectral measurements and only minimal course corrections are needed to keep the moon in the correct position relative to the wing pod aperture.

Prior to takeoff, the pilot applies power to the wing pod, causing both the IRIS and ARTEMIS computers to begin their start-up sequence. On boot, both computers automatically launch their respective control systems, with ARTEMIS occupying an idle state and the telescope resting in its stowed position within the pod. Fig. 1, pictured above, shows the air-LUSI instrument in the idle state. Immediately before takeoff, the pilot turns on the second pilot switch, commanding the IRIS control system to change to data acquisition mode.

Once the aircraft reaches the desired altitude and predetermined heading the third pilot switch is engaged, signaling the start of the target tracking sequence. The telescope then moves from its stowed position into its initial tracking position and acquires the Moon as a target. The lunar spectral irradiance is measured for up to 40 min,

Fig. 1. Design rendering of the autonomous robotic telescope mount instrument subsystem. This shows the final design structure that holds the actuators and telescope mount for the overall system. The system frame is designed to sit inside the ER-2 aircraft science pod with the telescope pointing out the top viewport.

after which the aircraft reaches the end of its tracking heading. At this point, the third switch is disengaged, which signals that the telescope be returned to its stowed position and idle state. After landing the pilot turns on the fourth switch which allows both computer systems to close out their running programs and gracefully shutdown before the power to the science pod is turned off.

3. Computer vision

A computer vision system is typically employed when dealing with automated target tracking problems. Common issues encountered with target detection are that the targets are generally small within the image, the target's orientation may vary from frame to frame, or their pixel information may not be overly distinct when compared to the background elements within the frame. Additional challenges result from having a non-static background, which implies that irrelevant information in an image cannot be removed to simplify detection processes. These issues are commonly reconciled by incorporating Pattern Matching or Key-Feature algorithms, where an initial image is saved as a reference and newly acquired images are compared to the original in the hopes of finding common elements [12,13].

In terms of target detection for the air-LUSI mission, acquiring the Moon as a target is the ideal scenario. To start, all flight campaigns and tracking sequences occur at night, which provides an all-black sky as a static background for the camera images. Additionally, it can be assumed that the Moon is the largest and brightest object in the camera frame, offering distinct contrast between the Moon and the background and a very obvious target for the control system. The homogeneity of the captured frames allows for the use of simplified and computationally inexpensive target detection algorithms.

A Basler (acA1920-40um) machine vision camera[1] was chosen as the data acquisition method for the robotic control system. At a high level, the images captured by the camera are sent to an image processing algorithm that is designed to calculate the pixel offset of the Moon from the center of the frame. This information is then sent to the line of sight controller as the measured state of the system, and compared against a predetermined pixel setpoint to produce an error signal. More on the determination of the pixel setpoint can be found in 4.

The image processing sequence is built primarily with the use of OpenCV, an open source computer vision and machine learning software library [24,25]. The processing begins with a frame capture from the camera, after which that frame is passed as a compressed image to an image processing subroutine. Once received, the image is filtered using a Gaussian Blur algorithm, and then a thresholding algorithm is applied. The initial compressed grayscale image represents a two dimensional array of pixels with each pixel having an assigned (0–255) eight bit value; where 255 represents white, and 0 represent black. By thresholding the image, eight bit limits are applied to the pixel values where anything below the limit is assigned a value of 0, and anything above the limit is assigned a value of 255. By applying thresholding, an abundance of irrelevant information is removed from the image while amplifying the contrast between target and background.

After thresholding is completed on the image, the Moon is pictured as a pure white circle on a perfectly black background. The image is then sent to a contouring algorithm that parses the image to find distinct shapes by assessing the limits of similarly valued pixels [24,25]. Although it is expected that the Moon is the only contour available in the image, a restriction is imposed on the image processing routine to only target the largest contour found in the sky.

Given all contouring information in the image, a minimum-area enclosing rectangle is fit to the Moon and provides information about the target center within the image frame. The final step in the image processing routine is to add a readout of the Moon location within the image frame and the desired location of the Moon as a setpoint. The pixel coordinates of the Moon in (x,y) is the primary input to the tracking controller and provides explicit information about the state of the system. Fig. 2 shows the final image after all thresholding, contouring, and readout processes have been performed.

4. Camera and telescope alignment

To ensure that the tracking system keeps the Moon centered within the field of view of the telescope, the tracking camera must be aligned with the telescope aperture. Since the tracking camera and telescope are viewing the Moon from two different vantage points, the camera frame and telescope aperture are not concentric. A pixel offset must be included in the setpoint coordinates so that the Moon is locked in the center of the telescope aperture during the tracking sequence, rather than the center of the tracking camera. It is expected that since the LoS of the tracking camera and telescope are collinear with respect to the azimuthal plane, the 'x' coordinate of the setpoint need not change, and only a 'y' offset is required.

The first step is to place the telescope at a known distance away from a bright light source. Next, the telescope steps across the light source in azimuth and elevation axes sequentially, as a spectrograph records the signal strength produced at each step. Calculating the centroid of the recorded signals on each axis gives the pixel coordinates (x,y) that correspond to the center of the telescope aperture at that specific distance between telescope and light source. By repeating this procedure at varying distances, a relationship can be established between distance to light source and required pixel offset. Extrapolating this relationship to infinity, as is the assumption when the telescope is viewing the moon, the exact 'y' pixel offset is determined. The resolution of the camera is 1920 pixels x 1200 pixels, corresponding to central frame pixel coordinates of (960, 600). The coordinates of the final setpoint (x,y) are then found by adding/subtracting the calculated pixel offset from the camera frame central coordinates.

5. Pointing controllers

5.1. Operating system and ROS framework

The ARTEMIS subsystem, responsible for controlling the tracking performance of the telescope, employs the Robotic Operating System (ROS) middleware on a Linux platform. ARTEMIS relies on a machine vision camera to determine the location of a target within a captured frame, and then passes the pixel coordinates to a PID control program [23,26].

[1] Certain commercial products are identified to specify the experimental study adequately. This does not imply endorsement by NIST or that the products are the best available for the purpose.

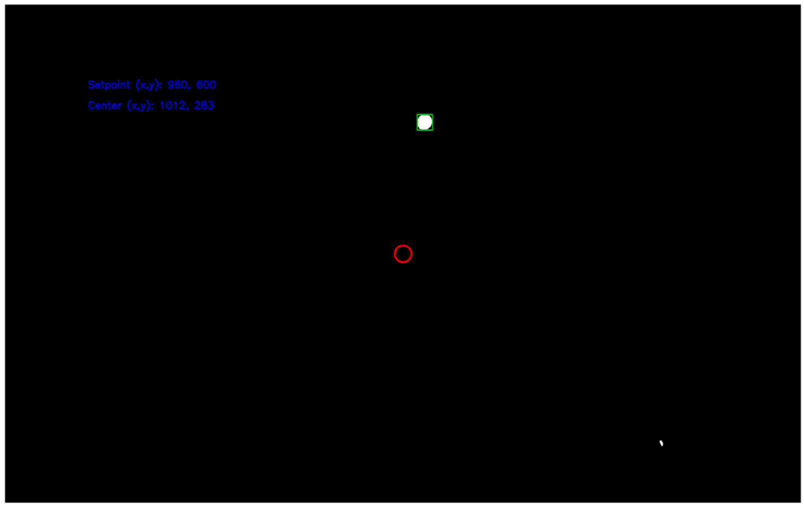

Fig. 2. Completely processed image. The green rectangle encloses the Moon, with the pixel coordinates of the rectangle center shown in blue text as "Center (x,y)". The red coincides with the center of the telescope, denoted in blue text as "Setpoint (x,y)".

The PID controller then calculates a control effort for each axis based on the distance separating the target from the setpoint. The control efforts are then passed to another program that manages all serial communications with the actuators. After the error signals are converted to an actuator piston movement, these commands are sent to the actuator thereby providing visual servoing of the system.

The ROS framework provides a robust platform on which to build the system and allows for a series of quasi-independent programs to run concurrently. The ROS middleware also provides a simple communication architecture between individual subroutines of the control system. Fig. 3 displays the general signal flow of the robotic control system, where the initial signal is provided by the tracking camera. Moving from left to right, the camera images are processed and the target information is passed on to the two independent controllers; one for each of the azimuth and elevation degrees of freedom. The controllers calculate a control signal that depends on the setpoint within the tracking camera images (detailed in Section 4), as well as the current position of the Moon's coordinates. The calculated control signal is then passed to the two independent actuator serial communication nodes which are responsible for issuing the new position commands to the linear actuators.

5.2. Line of sight controller

The control scheme for a double gimbal can be a very complicated multiple input multiple output system. To implement a fully rigorous control strategy the elevation and azimuth are not considered to be independent. Also, when using a camera as the input to a line of sight controller, movements in just the elevation or the azimuth do not produce a strictly horizontal or vertical adjustment in the camera's optical plane [12,13,15–17,27,28]. This results in a multiple input multiple output system where the pointing angle and tracking adjustments depend on both the kinematics and dynamics of the elevation and azimuth axes.

To simplify the control scheme for the air-LUSI instrument, a pair of closed loop controllers are used to treat the elevation and azimuth degrees of freedom as independent single input single output systems. Given an already established pixel setpoint which represents the desired location of the Moon within the tracking camera images, the incoming images are processed and the center pixel position of the target is determined [29–31]. In a sense, the camera provides a relative pixel distance measurement that separates the target from the desired position in (x,y). This state measurement is passed on to the independent controllers, which calculate separate control efforts that are then passed to their respective actuator [32–34]. Fig. 4 shows the line of sight feedback control loop that is used, and also represents the top and bottom paths of Fig. 3.

As the stroke positions were sent to the actuators, the pointing angle of the telescope was adjusted in elevation and azimuth. With each position adjustment the telescope and tracking camera were swept across the optical plane forcing the static pixel setpoint within the camera images to converge onto the target, producing a zero pixel error.

6. Network communications

The IRIS subsystem uses a rugged PC running Windows 7 and is responsible for electrically interfacing the air-LUSI instrument with the ER-2 aircraft and for capturing radiometric measurements of the Moon. The ARTEMIS subsystem uses a Linux OS and acquires tracking information from a machine vision camera in order to manage the pointing angle of the telescope. IRIS transitions between its operating states based on four pilot switches in the cockpit that are connected to the IRIS data acquisition system (DAQ). Based on the combination of engaged pilot switches (R1–R4), IRIS enters one of four states as seen in Fig. 5. If only R1 is engaged, air-LUSI occupies an idle state. When R1 and R2 are engaged, IRIS is capturing data but ARTEMIS is still idle. When all of R1, R2, and R3 are engaged ARTEMIS transitions to lunar tracking mode while IRIS is still capturing data. This is the state the entire air-LUSI instrument will occupy for the remainder of the flight until R3 is disengaged, bringing ARTEMIS back to its stowed position. To simplify communication and data exchange between subsystems, both computers transmit their operating states to one another in UDP status packets using the ER-2's onboard network. The IRIS-ARTEMIS subsystems are configured in a Master–Slave communication architecture, as such the ARTEMIS system only transitions states after receiving an IRIS status update as seen in Fig. 6.

To minimize the interdependency of the IRIS and ARTEMIS systems, a protocol that requires a persistent connection was not used. Instead, each instrument transmits current state over UDP at regular (one second) intervals. As the timing of the state changes is not critical, this design is tolerant to network errors and packet loss. The state messages are transmitted in JavaScript Object Notation (JSON) format, as it is human readable and nearly all modern programming languages have libraries available to serialize and deserialize to and from this format.

In addition to the subsystem communications between IRIS and ARTEMIS, both control computers forwarded UDP status updates to the aircraft NASA Airborne Science Data and Telemetry System (NASDAT).

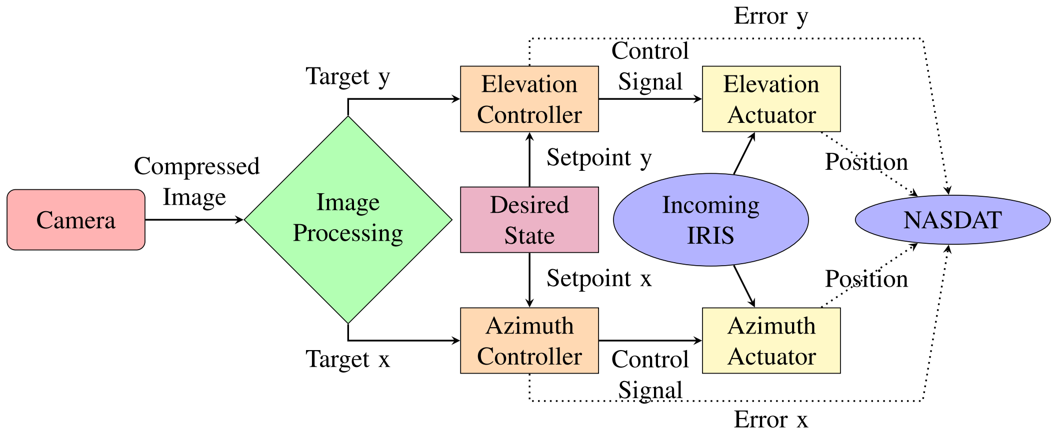

Fig. 3. Signal flow diagram for the autonomous robotic telescope mount instrument subsystem. Dotted lines represent outgoing status packets, namely the pixel error and actuator positions. Whereas the solid arrows show the transfer of control signals (such as target position, setpoint, and control effort) between modules of the robot. The ellipses represent interfaces that facilitate communication between subsystems and to the ground crew via the NASA-provided airborne science data and telemetry system.

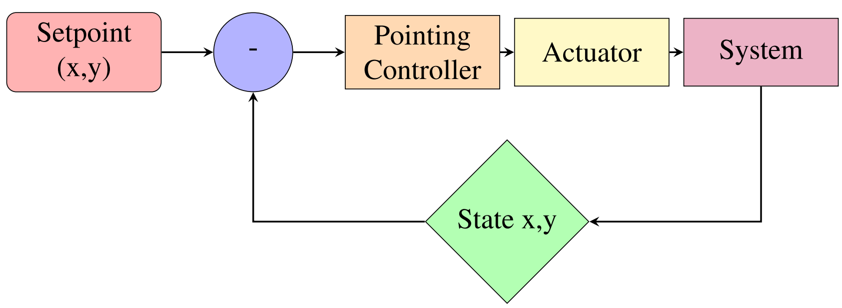

Fig. 4. Controller feedback loop for the telescope's line of sight.

The NASDAT is the airborne host NASA Airborne Science Program Sensor Network [35] for all of NASA science platforms and provides ethernet connections and satellite connectivity to airborne instruments. Each instrument transmits status packets containing comma-separated strings of instrument data to the NASDAT over ethernet at two different ports. The NASDAT then forwards these strings over Inmarsat and IRIDIUM to a server that NASA hosts, from which real-time, ground-based monitoring of instrument status can be performed. The NASDAT also permits remote connectivity via an encrypted connection directly to both the IRIS and ARTEMIS computers.

The ER-2 onboard network also provides a network time protocol (NTP) service to enable synchronization of the instrument logs to Universal Coordinated Time (UTC). The ARTEMIS computer uses a standard, open-source daemon to synchronize its clock, while the IRIS computer's clock is set before flight, and then a log is created to record the current offset between the NTP server and the onboard clock. This log is used to correct file times on recorded data if significant drift is observed, and drift does not affect instrument function.

7. System performance

From October 30th–November 19th of 2019, the air-LUSI science team deployed to NASA's Armstrong Flight research Center (AFRC) to complete the 2019 Demonstration Flight Campaign, consisting of five flights occurring between November 12th–17th. The 2019 Demonstration Flight Campaign was focused primarily on illustrating the capability of the instrument to reach its scientific goals, namely, collecting SI-traceable measurements of the lunar spectra with an absolute uncertainty of less than 1%. The following sections provide the tracking performance data from the 2019 Campaign, as well as presents some issues that were discovered in the field.

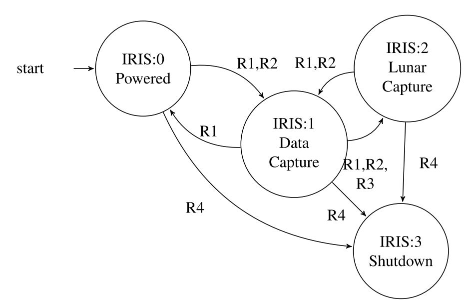

Fig. 5. State transitions for the irradiance instrument subsystem. Note that the ER-2 pilot engages the R1–R4 switches depending on the stage of the experiment.

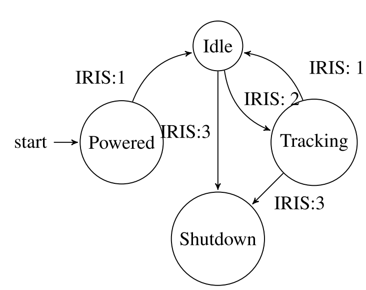

Fig. 6. State transitions for the autonomous robotic telescope mount instrument subsystem.

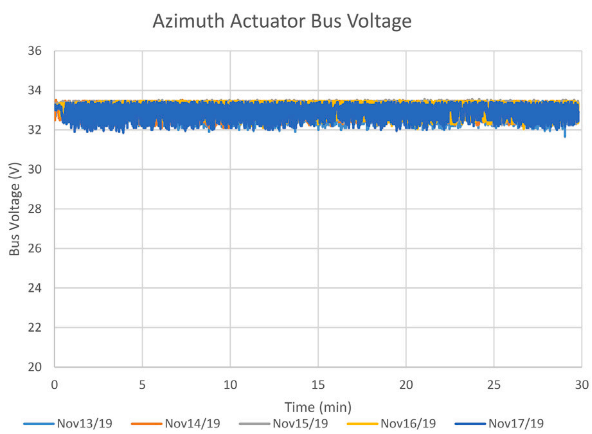

Fig. 7. Azimuth actuator bus voltage during flight.

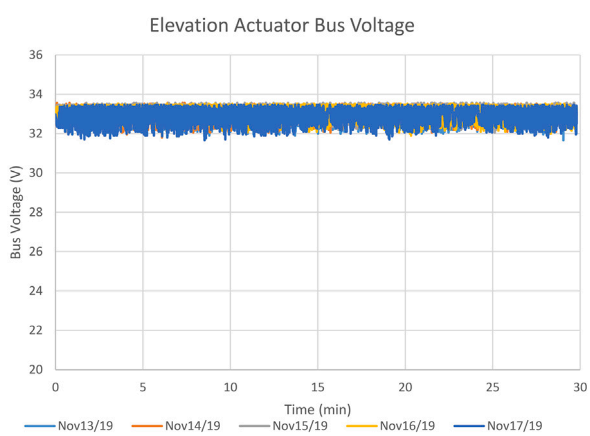

Fig. 8. Elevation actuator bus voltage during flight.

7.1. Actuator health & performance

For the 2019 Campaign, it was desired to monitor the real-time status of the elevation actuator. This was of particular importance because the elevation actuator was considered the highest risk to mission success. Having real-time data such as torque, position, and temperature allowed the mission control team to have eyes on this process and raise a red flag should something go askew. The below figures provide a high-level summary of the actuators health and performance during the five night flight campaign.

Figs. 7 & 8 show nothing but an entirely nominal bus (supply) voltage to the actuators over all five nights, given that the maximum operating bus voltage is 50 V. Figs. 9 & 10 illustrate the temperature dynamics of the actuators in flight. The operational temperature range of the actuators is between −40 °C and +80 °C [36], therefore one can draw the conclusion that both actuators were effectively protected against burn out.

Figs. 11 & 12 show the angle space range of motions that were achieved by the telescope during tracking. These plots are useful in determining if ARTEMIS was required to traverse to its physical limits, at which point control authority is lost. Based on the physical design of the instrument and geometric constraints within the science pod of the ER-2, it was found that the maximum range of motions for the azimuth and elevation axes are approximately ±15° and 75°, respectively.

For brevity, Figs. 13 & 14 show only the actuator torque profile for the November 14/2019 flight. The red lines on the plots indicate

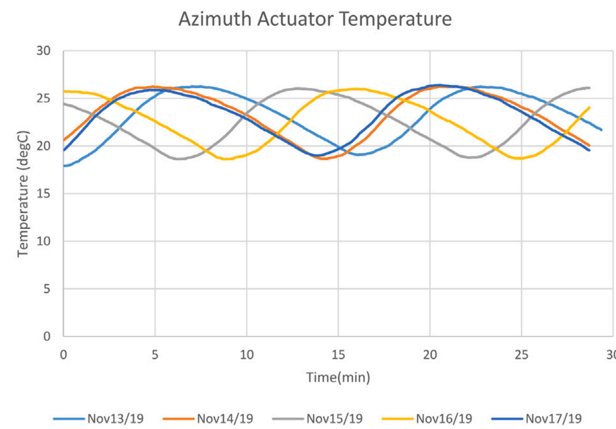

Fig. 9. Azimuth actuator temperature during flight.

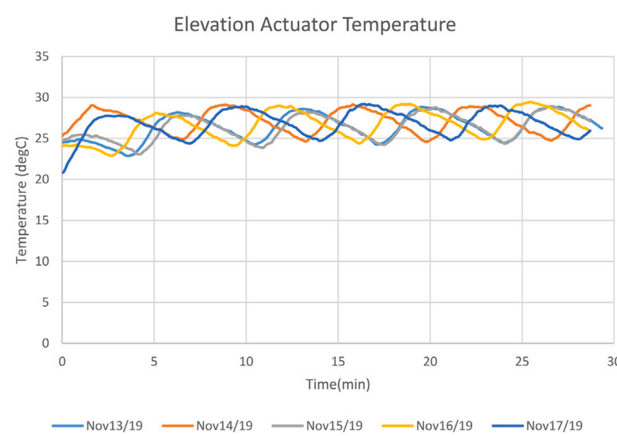

Fig. 10. Elevation actuator temperature during flight.

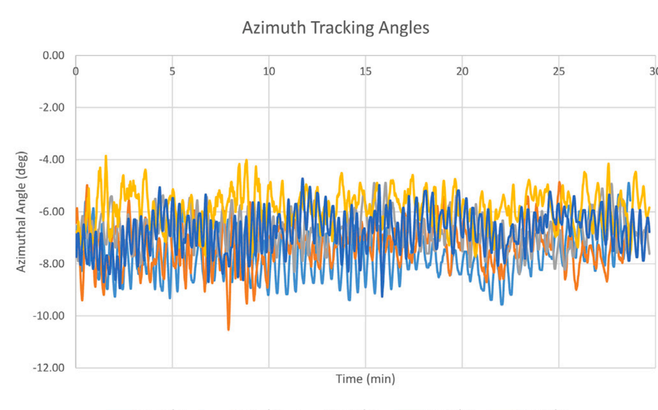

Fig. 11. Azimuth actuator range of motion during flight.

the maximum allowable *continuous* torque, in arbitrary actuator units. Fig. 14 shows a consistent overshoot on this parameter, which is cause for some concern. However, this plot is actually displaying is the *instantaneous* torque in the actuator, which is flipping between minima and maxima as can be seen more clearly in Fig. 13. The maximum instantaneous torque of the actuator corresponds to a value of 28 000, which was not even remotely approached. It should be noted that the intense flipping behavior of the torque signal is a direct result of an overloaded actuator. Continued operation in this load regime will lead to increased wear and tear and drastically reduce actuator life.

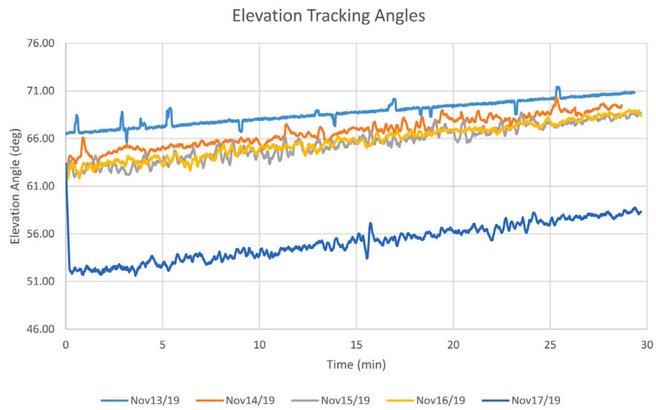

Fig. 12. Elevation actuator range of motion during flight.

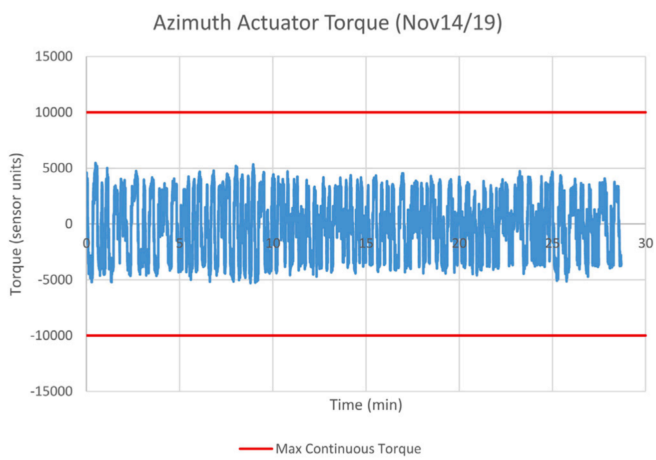

Fig. 13. Azimuth actuator applied torque during flight.

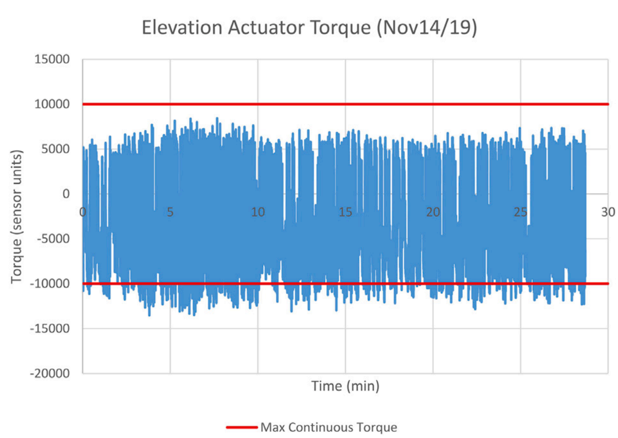

Fig. 14. Elevation actuator applied torque during flight.

7.2. Target tracking performance

To measure the accuracy of ARTEMIS, the tracking error was evaluated by the (x,y) pixel offset in the machine vision camera frame, with the total tracking error represented by the radial offset between the Moon center and the pixel setpoint. For the particular camera and lens combination used on the ARTEMIS, the conversion from pixel space to angle space is (0.053°/pixel). This conversion factor was then applied to the pixel offset data such that the air-LUSI team could determine whether or not ARTEMIS was satisfying the less than 0.5° offset requirement. The plots below illustrate the tracking accuracy of the ARTEMIS, however in the interest of brevity only the tracking data from November 14/2019 is displayed.

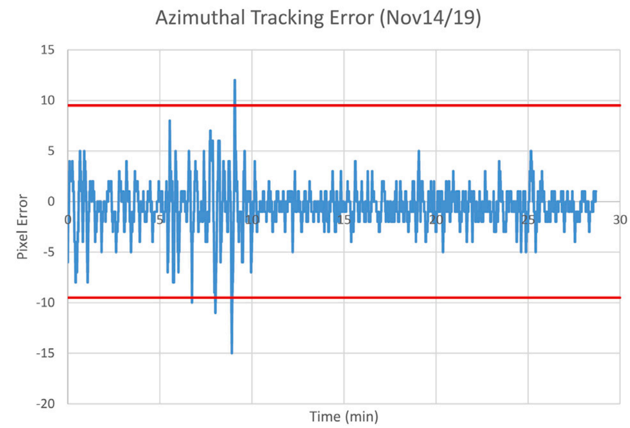

Fig. 15. Azimuthal pixel error during flight.

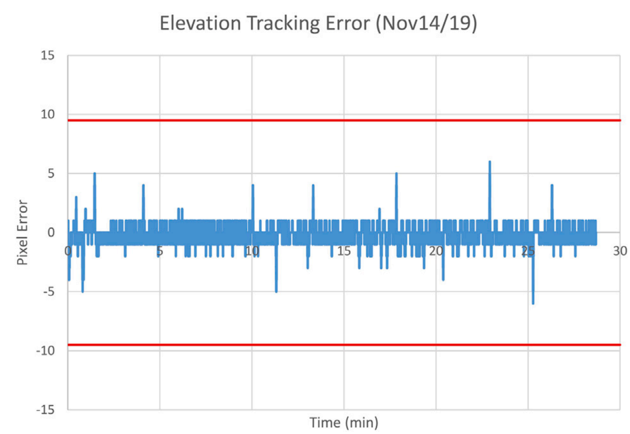

Fig. 16. Elevation pixel error during flight.

Table 1
Defining the different regimes of tracking accuracy.

Degree of accuracy	Total tracking error (degrees)
Excellent	0 <= Error < 0.125
Good	0.125 <= Error < 0.25
In Spec	0.25 <= Error < 0.5
Off Target	0.5 <= Error

Figs. 15 & 16 are displaying the pixel error in the azimuthal and elevation axes, respectively. Interestingly, the elevation actuator, which was the expected culprit of the mission, shows excellent tracking behavior whereas the azimuthal axis is certainly under performing. Fig. 17 is the absolute, or radial, offset from the Moon center to the pixel setpoint. It can be seen that there were only a handful of instances in which the telescope was completely off target, however, Fig. 18 on the following page serves the purpose of providing some context.

Fig. 18 shows the percentage of lunar tracking time that was spent occupying different regimes of accuracy, which are defined in Table 1. It can be seen that even though Fig. 17 shows several off target measurements, Fig. 18 illustrates that these off target measurements only represent 0.4% of the tracking window, and can likely be pin pointed and filtered out. Table 2 below is a concise summary of the tracking data across all five nights.

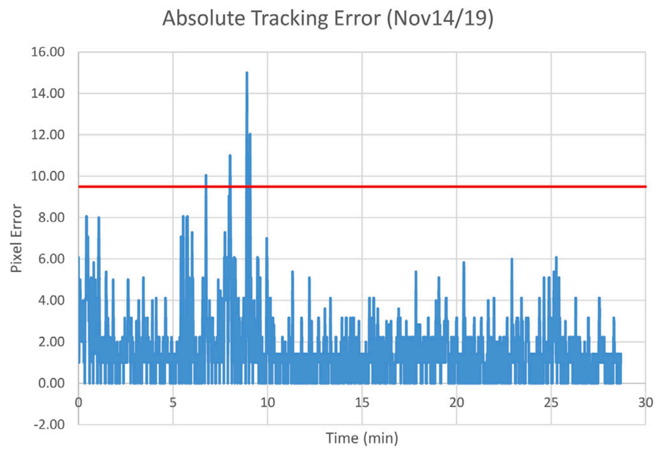

Fig. 17. Total pixel error during flight.

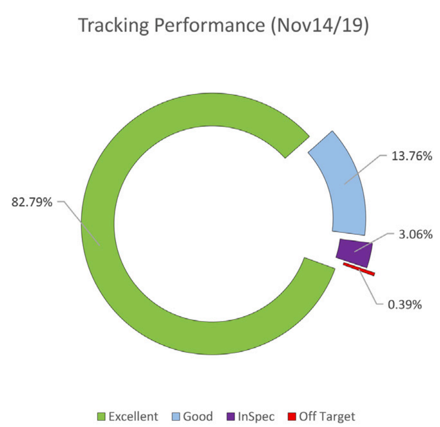

Fig. 18. Time spent in different accuracy regimes (%).

Table 2
Summary of demonstration flight campaign tracking statistics.

Accuracy	Flight				
	Nov 13/19	Nov 14/19	Nov 15/19	Nov 16/19	Nov 17/19
Excellent	76.40%	82.79%	85.74%	83.75%	72.48%
Good	22.01%	13.76%	13.91%	13.31%	23.45%
In Spec	1.54%	3.06%	0.32%	2.91%	3.60%
Off Target	0.05%	0.39%	0.03%	0.03%	0.38%
RMSE (deg)	0.11	0.11	0.10	0.11	0.13

7.3. Demonstration flight Campaign review

The Moon occupied elevation angles of nearly 61° to 71° during flight times, a significant increase from the 50° to 55° angle space encountered in the 2018 Engineering Flights [37]. From a scientific standpoint, performing these measurements at maximal Moon elevation is ideal since there is less atmosphere for the photons to travel through when the Moon is high in the sky. However, from an engineering stand point, this not only increases the stress on the robotic control system but also greatly reduces the control authority as the current design is optimized for field of view in the 47° to 55° elevation angle space. In other words, as the elevation angle increases, the reachable sight lines of the telescope in the azimuth are greatly reduced. If the team wishes to continue these experiments at near vertical elevation angles, some mechanical redesign of the control system should be explored.

The tracking performance in the azimuthal axis also raised some questions early on in the Campaign. It was discovered that there was a bug in the flight software where the azimuth actuator was receiving the same acceleration and velocity parameters for the trajectory generation software as the elevation actuator. The elevation actuator's acceleration and max velocity parameters were greatly reduced to limit the current drawn by this over loaded motor. The elevation actuator parameters were Acceleration = 100 (arbitrary units) and Velocity = 30 000 (arbitrary units), which proved effective in flight as the elevation actuator only needs to correct for changes in the roll attitude of the aircraft – a fairly stable axis. The azimuth actuator needs to correct for changes in both Yaw and Pitch of the aircraft, which are far more dynamic. The azimuth actuator was grossly underpowered for the Demonstration Flight Campaign as it should have used an Acceleration = 2000 and Velocity = 60 000, based on laboratory and field tests conducted between June and August of 2019. It can also be seen from Fig. 13 that the instantaneous torque never climbed past 5000 (arbitrary units), thereby indicating that the aforementioned acceleration and velocity parameters can be safely implemented.

Following the review of the first campaign, air-LUSI received a number of hardware and software upgrades to address the areas of risk discovered in the 2018 Engineering Flights. These upgrades were proven to work during the subsequent 2019 Demonstration Flight Campaign, in which ARTEMIS tracked the Moon with an RMSE tracking accuracy of (0.11°).

8. Conclusion

The air-LUSI instrument was deployed on its first Engineering Flight Campaign on August 1st 2018 and tracked the Moon with an RMSE tracking accuracy of (0.059°). It was deployed again for a 2019 Demonstration Flight Campaign, in which ARTEMIS tracked the Moon with an RMSE tracking accuracy of (0.11°). The stability of the tracking system during these deployments enabled the first ever measurements of the lunar spectral irradiance from a high-altitude platform.

To simplify the electrical integration of the air-LUSI instrument to the ER-2 aircraft, only IRIS was physically connected to the ER-2 and could interpret signals from the cockpit. By only electrically connecting a single subsystem to aircraft the air-LUSI team used the ER-2 network to subordinate the ARTEMIS subsystem to the IRIS subsystem. When the pilot would flip a switch in the cockpit to initiate a change in functionality, the IRIS DAQ would register a high signal and respond by changing its state. By sending its state using UDP status packets to the ARTEMIS system, IRIS would command ARTEMIS to change its states accordingly.

The naive approach of treating the two axes of the telescope gimbal as independent by using two single input single output controllers proved effective and simplified the control of a complicated system. Although treated independently, the two closed loop controllers for azimuth and elevation axes compensated for any errors resulting within the systems and produced tracking accuracy that exceeded the design team's expectations.

Radiometric characterization of the telescope is ongoing. The air-LUSI instrument is expected to be used throughout the coming years to compile lunar irradiance datasets for a wide range of lunar phases relevant to satellite calibration. Given enough data, a highly accurate lunar spectral irradiance model can be produced and allow for higher accuracy monitoring of our planet based on a lunar calibration of earth observing satellites.

Acknowledgments

We are grateful to the staff at NASA's Armstrong Flight Research Center (AFRC) in Palmdale, California for enabling the success of this project. We are also thankful for the support provided by the staff at NIST and NASA headquarters. This work was partially funded under the NASA Airborne Instrument Technology Transfer Program via Grant NNX17AL25G titled: Development of a Highly Accurate Lunar Spectral Irradiance Measurement Capability, The Airborne LUnar Spectral Irradiance Instrument (air-LUSI); as well as by the Natural Sciences and Engineering Research Council of Canada and the University of Guelph.

Declaration of competing interest

No author associated with this paper has disclosed any potential or pertinent conflicts which may be perceived to have impending conflict with this work. For full disclosure statements refer to https://doi.org/10.1016/j.actaastro.2020.07.004.

References

[1] J. Anderson, K. Becker, H. Kieffer, D.N. Dodd, Real-time control of the robotic lunar observatory telescope, Publ. Astron. Soc. Pac. 111 (760) (1999) 737–749.
[2] C.E. Cramer, K.R. Lykke, J.T. Woodward, A.W. Smith, Precise measurement of lunar spectral irradiance at visible wavelengths, J. Res. Natl. Inst. Stand. Technol. 117 (1) (2013) 737–749.
[3] A. Smith, S. Lorentz, T. Stone, R. Datla, Lunar spectral irradiance and radiance (LUSI): New instrumentation to characterize the moon as a space-based radiometric standard, J. Res. Natl. Inst. Stand. Technol. 117 (1) (2012) 185–201.
[4] S. Miller, R. Turner, A dynamic lunar spectral irradiance data set for NPOESS/VIIRS day/night band nighttime environmental applications, IEEE Trans. Geosci. Remote Sens. 47 (7) (2009) 2316–2329.
[5] I. Grant, H. Kieffer, T. Stone, J. Anderson, Lunar calibration of the GMS-5 visible band, in: Proceedings of 2001 IEEE International Geoscience and Remote Sensing Symposium (IGARSS), IEEE, Publisher address, 2001, pp. 1–3.
[6] H. Kieffer, T. Stone, The spectral irradiance of the moon, Astron. J. 129 (6) (2005) 2887–2901.
[7] A. Cataford, S.A. Gadsden, K. Turpie, Air-LUSI: A robotic telescope design for lunar spectral measurements, Adv. Space Res. 65 (10) (2020) 2315–2323.
[8] B. Cook, D. Braun, S. Hankins, J. Keonig, D. Moore, Precision linear actuator for space interferometry mission (SIM) siderostat pointing, in: 39th Aerospace Mechanisms Symposium, 2008.
[9] e.a. B. Cook, Precision linear actuator for space interferometry mission (SIM) siderostat pointing, in: Proceedings of the 39th Aerospace Mechanisms Symposium, Jet Propulsion Laboratory, Jet Propulsion Laboratory and National Aeronautics and Space Administration, Pasadena, CA, 2008, pp. 8458–8463.
[10] e.a. R. Saulescu, On the eccentricity effects in solar tracking triangular linkage with eccentric linear actuator, in: Proceedings of the 39th Aerospace Mechanisms Symposium, IEEE, Publisher address, 2007, pp. 8458–8463.
[11] A. Cataford, S.A. Gadsden, K. Turpie, Air-LUSI: Autonomous telescope design for lunar spectral irradiance measurements, in: 2019 SPIE Advanced Optics for Imaging Applications: UV Through LWIR IV, SPIE, 2019.
[12] Z. Hurak, M. Rezac, Image-based pointing and tracking for inertially stabilized airborne camera platform, IEEE Trans. Control Syst. Technol. 20 (5) (2012) 1146–1159.
[13] Z. Hurak, M. Rezac, Combined line-of-sight inertial stabilization and visual tracking: Application to an airborne camera platform, in: Proceedings of the 48th IEEE Conference on Decision and Control and 28th Chinese Control Conference, vol. 1, IEEE, Publisher address, 2009, pp. 8458–8463.
[14] J. Chittle, M. Biglarbegian, S.A. Gadsden, Mobile robot tracking using an overhead camera and sensor fusion, in: 2018 IEEE Canadian Conference on Electrical and Computer Engineering (CCECE), 2018.
[15] J.M. Hilkert, Inertially stabilized pltaform technology, IEEE Control Syst. Mag. 28 (1) (2008) 26–46.
[16] J. Osborne, G. Hicks, R. Fuentes, Global analysis of the double-gimbal mechanism, IEEE Control Syst. Mag. 28 (4) (2008) 44–64.
[17] M. Masten, Inertially stabilized platforms for optical imaging systems, IEEE Control Syst. Mag. 28 (1) (2008) 47–64.
[18] H. Wang, T. Williams, Strategic inertial navigation systems, IEEE Control Syst. Mag. 28 (1) (2008) 65–85.
[19] H. Kaercher, P. Eisentraeger, K. Wandner, R. Nordmann, U. Schoenhoff, The pointing control system for the stratospheric observatory for infrared astronomy SOFIA, in: Proceedings of SPIE 3351, Telescope Control Systems III, 1998.
[20] N. Fiebig, H. Jakob, E. Pfuller, H.-P. Roser, M. Wiedemann, J. Wolf, Evolution of the SOFIA tracking control system, in: Proceedings of SPIE 9152, Software and Cyberinfrastructure for Astronomy III, 2014.
[21] K. Wandler, H. Kaercher, Pointing control system of SOFIA, in: Proceedings of SPIE 4014, Airborne Telescope Systems, 2000.
[22] J. Park, L. Bahn, C. hun Lee, T. il Kim, K. soo Kim, D. il Cho, A novel method for vision tracking with line of sight control using a fuzzy logic controller and Euler angle orientation in the feedforward loop, in: IEEE 8th International Conference on Ubiquitous Robots and Ambient Intelligence (URAI), 2011.
[23] W. Bolton, Mechatronics: Electronic Control Systems in Mechanical and Electrical Engineering, fifth ed., Pearson, United States of America, 2011.
[24] OpenCV Team, About – opencv, 2019, https://opencv.org/about/ Online; (Accessed 27 September 2019).
[25] G. Bradski, The opencv library, Dr. Dobb's J. Softw. Tools (2000).
[26] W. Bolton, Control Engineering, second ed., Pearson, Edinburgh Gate Harlow Essex England, 1998.
[27] J. Ranganathan, W. Semke, Three-axis gimabl surveillance algorithms for use in small UAS, in: Proceedings of 2008 ASME International Mechanical Engineering Congress and Exposition (IMECE), ASME, Publisher address, 2008, pp. 1–10.
[28] A. Tatoglu, C. Campana, Adaptive gimbal control approach to account for power consumption and landmark tracking quality, in: Proceedings of 2016 ASME International Mechanical Engineering Congress and Exposition (IMECE), ASME, Publisher address, 2016, pp. 1–8.
[29] A. Qadir, W. Semke, J. Neubert, Vision based neuro-fuzzy controller for a two axes gimbal system with small UAV, J. Intell. Robot. Syst. 74 (3–4) (2014) 99–112.
[30] F. Chaumette, P. Rives, B. Espiau, Positioning of a robot with respect to an object, tracking it and estimating its velocity by visual servoing, in: Proceedings of the 1991 IEEE International Conference on Robotics and Automation, IEEE, 1991, pp. 2248–2253.
[31] J. Schrimpf, M. Lind, G. Mathisen, Time analysis of a real-time sensor-servoing system using line-of-sight path tracking, in: Proceedings of the 2011 IEEE International Conference on Intelligent Robots and Systems, IEEE, 2011, pp. 2861–2866.
[32] J. Okamoto, V. Grassi, Visual servo control of a mobile robot using omnidirectional vision, in: Proceedings of Mechatronics, University of Twente, 2002, pp. 413–422.
[33] J. Park, W. Hwang, H. Kwon, K. Kim, A novel line of sight control system for a robot vision tracking system, using vision feedback and motion-distrubance feedforward compensation, Robtica 31 (1) (2013) 99–112.
[34] Y.-S. Shiao, Design and implementation of real-time tracking system based on vision servo control, Tamkang J. Sci. Eng. 4 (1) (2001) 45–58.
[35] A. Misc, NASA airborne science data and telemetry tystem, 2017, On the WWW URL https://asapdata.arc.nasa.gov/sensors/nasdat.html.
[36] Ultramotion Technical Staff, Ultramotion Servocylinder Information and User Manual Version, A.07, Ultramotion Inc, Cutchogue, New York, 2017.
[37] A. Cataford, air-LUSI: The Mechanical and Control System Design of NASA's Airborne Lunar Observatory, University of Guelph, 2018.